Solid State Nuclear Magnetic Resonance 84 (2017) 89–102

Contents lists available at ScienceDirect

Solid State Nuclear Magnetic Resonance

journal homepage: www.elsevier.com/locate/ssnmr

Trends

Investigating FAM-N pulses for signal enhancement in MQMAS NMR of quadrupolar nuclei

Henri Colaux, Daniel M. Dawson, Sharon E. Ashbrook*

School of Chemistry, EaStCHEM and Centre of Magnetic Resonance, University of St Andrews, North Haugh, St Andrews KY16 9ST, UK

ARTICLE INFO

Keywords:
Solid-state MAS NMR spectroscopy
MQMAS
Quadrupolar nuclei
Fast-amplitude modulation
FAM-N pulses
Challenging systems

ABSTRACT

Although a popular choice for obtaining high-resolution solid-state NMR spectra of quadrupolar nuclei, the inherently low sensitivity of the multiple-quantum magic-angle spinning (MQMAS) experiment has limited its application for nuclei with low receptivity or when the available sample volume is limited. A number of methods have been introduced in the literature to attempt to address this problem. Recently, we have introduced an alternative, automated approach, based on numerical simulations, for generating amplitude-modulated pulses (termed FAM-N pulses) to enhance the efficiency of the triple- to single-quantum conversion step within MQMAS. This results in efficient pulses that can be used without experimental reoptimisation, ensuring that this method is particularly suitable for challenging nuclei and systems. In this work, we investigate the applicability of FAM-N pulses to a wider variety of systems, and their robustness under more challenging experimental conditions. These include experiments performed under fast MAS, nuclei with higher spin quantum numbers, samples with multiple distinct sites, low-γ nuclei and nuclei subject to large quadrupolar interactions.

1. Introduction

Many of the nuclei of interest in inorganic chemistry, mineralogy and materials science, and ~75% of the magnetically-active nuclides in the Periodic Table, are quadrupolar, *i.e.*, possess a nuclear spin quantum number $I > 1/2$ [1–3]. In addition to the anisotropic broadening this produces, many of these nuclei also have low γ, low natural abundance or low chemical abundance in the system under study, resulting in considerable experimental challenges. Unlike their spin I=1/2 counterparts, magic-angle spinning (MAS), *i.e.*, rapid rotation of the sample around an axis inclined at 54.736° to the external magnetic field, B_0, is not able to completely remove the anisotropic broadening and produce high-resolution spectra for quadrupolar nuclei, no matter how rapid the sample rotation [1–3]. A number of approaches have been taken to enable the removal of the second-order quadrupolar broadening, including the composite sample spinning techniques, dynamic angle spinning (DAS) [3,4] and double rotation (DOR) [3,5]. However, the requirement for dedicated hardware has limited the wider applicability and popularity of these techniques. In contrast, the multiple-quantum (MQ) MAS experiment, introduced by Frydman and Harwood in 1995 [3,6], enables high-resolution NMR spectra for quadrupolar nuclei to be obtained using only conventional hardware. This two-dimensional experiment (performed under MAS conditions) involves the correlation of multiple-quantum coherences (typically triple-quantum coherences, *i.e.*, $m_I=+3/2 \leftrightarrow m_I=-3/2$) in t_1 with the central transition (CT), *i.e.*, $m_I=+1/2 \leftrightarrow m_I=-1/2$, in t_2, exploiting the similarity in form, but not in the magnitude, of the quadrupolar broadening of the two transitions. A number of different experimental approaches have been suggested, with early effort focussed on the acquisition of purely-absorptive lineshapes [7–10]. MQMAS has gained widespread popularity and has been applied to a variety of materials.

The main drawback of MQMAS is its poor sensitivity, which results from the inefficient excitation and conversion of triple-quantum coherences, a process that is forbidden by the conventional quantum selection rules, but becomes allowed in the presence of a significant quadrupolar interaction. There have been a number of investigations into the optimum pulse durations for multiple-quantum filtration, and how these are affected by a variety of experimental conditions [7,11–13]. The efficiency of this filtration increases with the radiofrequency (rf) field strength of the pulses; however, this is also limited for low-γ nuclei [13]. In an attempt to overcome the problems with sensitivity, Gan introduced the satellite-transition (ST) MAS experiment [14]; conceptually similar to MQMAS, but involving the correlation of purely single-quantum satellite (*i.e.*, $m_I= \pm 1/2 \leftrightarrow m_I= \pm 3/2$) transitions with the central transition. Despite its significant sensitivity advantage,

* Corresponding author.
E-mail address: sema@st-andrews.ac.uk (S.E. Ashbrook).

http://dx.doi.org/10.1016/j.ssnmr.2017.01.001
Received 14 October 2016; Received in revised form 5 January 2017; Accepted 10 January 2017
Available online 18 January 2017

STMAS is more challenging to implement, requiring a very accurate setting of the rotation axis and a very stable spinning rate [14,15]. Consequently, this experiment has not matched the popularity of MQMAS, but has successfully been exploited for systems or nuclei with low sensitivity or to detect the presence of μs-timescale dynamics [16–18]. As a result, there has been considerable attention focussed on improving the sensitivity of the MQMAS experiment, with most research focussed on developing and improving the conversion pulse, *i.e.*, the pulse that converts triple-quantum to central-transition coherences [8–10]. Approaches considered include SPAM (soft-pulse added mixing) [19,20], DFS (double frequency sweep) [21], FAM (fast amplitude modulation) [22–24] and HS (hyperbolic secant) pulses [25], which have been compared and contrasted in a range of studies [19–27]. Some work has also attempted to improve either the efficiency of the excitation pulse or its ability to uniformly excite a powder lineshape. These include RIACT (rotor-induced adiabatic coherence transfer) [28], FASTER (fast spinning gives transfer enhancement at rotary resonance) [29], SFAM (shifted fast-amplitude modulation) [30] and optimal control theory [31]. In addition, MQMAS experiments can be combined with CPMG (Carr-Purcell-Meiboom-Gill) pulse trains for further sensitivity gains [32–34]. Although combination of MQMAS with cross polarisation (CP) has been demonstrated, this is typically used for spectral editing as signal enhancements are rarely obtained using CP for quadrupolar nuclei, owing to the more complex spin dynamics involved [35,36].

The FAM and DFS approaches are perhaps those most commonly employed for sensitivity enhancement of MQMAS experiments, owing to their relative ease of implementation and the signal improvements they produce. DFS comprises the application of a modulated rf pulse, where the frequency is swept during a time τ_p [21]. The aim of such a pulse is to saturate or invert the satellite transitions, thereby transferring triple- to single-quantum coherences. In reality, both processes probably occur depending on the crystallite orientation, the magnitude of the quadrupolar interaction (C_Q) and the MAS rate (ν_R). FAM pulses aim to execute similar coherence transfers to DFS but use a series of rectangular pulses (thereby being easier to implement on earlier software). A number of different types of FAM pulses are available, and both "windowed" and "windowless" versions have been used [8–10,22–24]. FAM-I pulses consist of repeating blocks of uniform pulses (and intervals) and experimental optimisation requires the pulse/interval duration and the number of repeat blocks to be varied. In FAM-II the pulses used vary in duration (typically decreasing as the number of pulses increases). Optimisation of FAM-II-type pulses is typically carried out experimentally, by considering the duration of each pulse sequentially. The experimental optimisation of such composite pulses can be very challenging and time consuming, particularly when the sensitivity is low (*i.e.*, for the very cases where such pulses are vital), and for FAM-II this either limits the number of pulses used practically, or requires some restriction where earlier pulses in the sequence are not re-optimised upon addition of subsequent pulses. Recently, we have demonstrated the use of a fast and efficient automated optimisation procedure that enables the optimum number and duration of the components of a FAM pulse to be determined using numerical simulation software, producing a so-called "FAM-N" pulse, *i.e.*, a pulse with N sequential but oppositely-phased components [37]. Unlike previous work [24,38], there is no constraint on the relative lengths or efficiencies of the individual pulses, and the last pulse in the sequence is reoptimised automatically when the next oppositely-phased pulse is added.

Previously, we have shown that FAM-N pulses can be generated easily and efficiently, produce good signal enhancements and typically can be used without experimental reoptimisation [37]. The pulses were shown to perform consistently, and significantly, better than single-pulse conversion and outperformed SPAM and FAM-I pulses for the model system studied. Signal enhancements were typically better than FAM-II (with the exception of cases where the optimisation procedure produced a FAM-N pulse with two components), and were similar to those achieved using DFS [37]. The best FAM-N enhancements were achieved when the pulses were generated with some prior knowledge of the experimental parameters (*e.g.*, rf field strength or MAS rate) or those associated with the nucleus (*e.g.*, C_Q and asymmetry (η_Q) of the quadrupolar interaction), although it was shown that the pulses appear robust with respect to reasonable variation of the experimental parameters [37]. Therefore, even when the user has little prior knowledge of the system under study, reasonably good enhancements can be obtained through the use of an approximate value of C_Q (*e.g.*, estimated from, or at least limited by, the linewidth in the MAS spectrum). The pulses also resulted in good enhancements when they were applied with rf field strengths that varied by a few tens of kHz from those with which they were simulated [37]. Furthermore, it was shown that only a small improvement in efficiency was obtained if the FAM-N pulse generated was reoptimised experimentally, either by varying the total duration (*i.e.*, scaling each of the components by the same proportion), varying the duration of one or more of the components or, perhaps more practically, by optimising the rf field strength with which it is applied. Most previous work was focused on a model system [37], ^{87}Rb (I=3/2) NMR of $RbNO_3$, a material with three distinct Rb species, but where the quadrupolar parameters are known and are also very similar to each other [39]. In this work, we extend the investigation to include the application of FAM-N pulses to nuclei with high spin quantum number, materials with multiple distinct (and very different) sites, nuclei with low γ or low abundance and nuclei subject to a significant quadrupolar interaction. We also investigate the efficiency and robustness of this approach for experiments carried out at fast MAS rates. The aim is to demonstrate that this conceptually simple approach can be applied to "real" and challenging systems, where sensitivity enhancement is a necessity rather than just a welcome gain.

2. Experimental details

FAM-N pulses were generated using the high-throughput optimisation procedure, described in Ref. [37], which calls the density matrix simulation program SIMPSON [40] from an in-house MATLAB [41] script. User-inputted parameters include the external magnetic field strength (B_0), the MAS rate (ν_R), the inherent radiofrequency nutation rate (ν_1) and the quadrupolar parameters ($C_Q=eQV_{zz}/h$ and $\eta_Q=(V_{xx}-V_{yy})/V_{zz}$)). The procedure optimises the transfer efficiency of a unit amount of symmetrical triple-quantum coherences (*i.e.*, density matrix element {1, 4} for I=3/2 or {2, 5} for I=5/2, *etc.*,) to central-transition (CT) single-quantum coherences of the same sign (*i.e.*, density matrix element {2, 3} for I=3/2 or {3, 4} for I=5/2, *etc.*,). The composite pulse produced can be written directly into the pulse program for a split-t_1 shifted-echo triple-quantum MQMAS experiment [42] (see Fig. 1) in place of the conversion pulse and, in this work, is used directly in the experiment without any reoptimisation. The optimisation procedure is shown schematically in Fig. 1c. The amount of CT single-quantum coherence generated is monitored as the duration of a high-power rf pulse is varied. The duration of the first pulse is fixed at that producing the maximum coherence transfer, and a second pulse is then applied with inverted phase. The duration of this pulse is incrementally varied. The duration of the first pulse is then increased and the variation of the second pulse is repeated. This procedure is carried out a number of times until additional increments decrease the maximum coherence transfer. At this point an additional pulse is added, again with inverted phase. This procedure is repeated, generating a series of pulses with opposite phase and varying duration. The optimisation procedure is terminated when adding the next pulse does not increase the maximum conversion efficiency.

Experimental NMR spectra were acquired using Bruker Avance III spectrometers equipped with 9.4 T (University of St Andrews, UK), 14.1 T (University of St Andrews, UK), 18.8 T (Université de Lille 1, Lille, France) or 20.0 T (UK Solid-State NMR Facility, Warwick, UK)

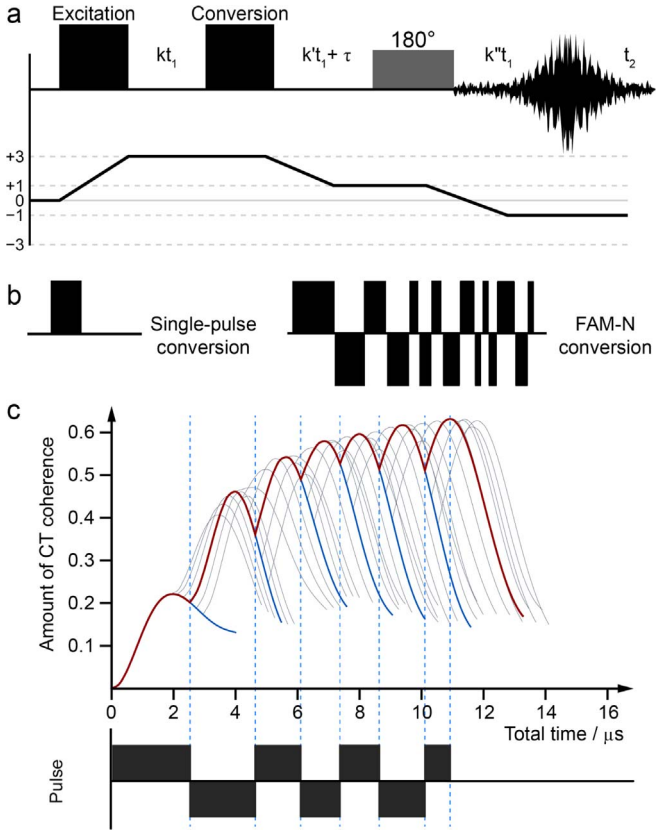

Fig. 1. (a) Pulse sequence and coherence transfer pathway for a split-t_1 shifted-echo MQMAS experiment. (b) Schematic representation of conventional (*i.e.*, single) and FAM-N conversion pulses. (c) Schematic showing the result of a FAM-N optimisation for ^{23}Na (I=3/2) at B_0=14.1 T (ν_0=158.8 MHz), with ν_1=80 kHz and ν_R=12.5 kHz, with the evolution of the amount of CT single-quantum coherence plotted as a function of time and of the pulse used in the simulation. Grey lines show the amount of CT single-quantum coherence for all of the intermediate optimisation steps, the blue line are for the optimisations steps that were used for the subsequent steps of the FAM-N optimisation. The red line shows the evolution of the amount of CT single-quantum coherence for the final FAM-N pulse.

magnets. Further details on the MAS rates used and the rf field strengths applied can be found in the relevant figure captions and in the Supporting Information. Chemical shift scales are shown in ppm, referenced relative to 0.1 M NaCl (aq), 11 M $MgCl_2$ (aq), 1.1 M $Al(NO_3)_3$ (aq), 0.1 M KCl (aq), 0.06 M $Sc(NO_3)_3$ (aq), 0.01 M RbCl (aq) and $K[NbCl_6]$ in CH_3CN for ^{23}Na, ^{25}Mg, ^{27}Al, ^{39}K, ^{45}Sc, ^{87}Rb and ^{93}Nb, respectively. Reference shifts were determined using secondary references of NaCl (s) at δ_{iso}=7.9 ppm [43], MgO (s) at δ_{iso}=26 ppm [44], $Al(acac)_3$ (s) at δ_{iso}=0 ppm [45], KBr (s) at δ_{iso}=55.2 ppm [1], $LaScO_3$ (s) at δ_{iso}=162 ppm [46], RbCl (s) at δ_{iso}=128 ppm [1], and $LiNbO_3$ (s) at δ_{iso}=−1004 ppm [47]. Two-dimensional triple-quantum MAS experiments were recorded using a phase-modulated split-t_1 shifted-echo pulse sequence [42], with selection of the +3→+1→−1 coherence transfer pathway, as shown in Fig. 1a, and varying the values of k, k' and k" depending on the spin quantum number of the nucleus studied. The final pulse is a CT-selective inversion pulse. The indirect dimension is referenced according to the convention described in Ref. [48].

3. Results and discussion

3.1. Applications to nuclei with high spin quantum number

It was shown in previous work [37], both in experiment and in simulation, that for I=3/2 nuclei the efficiency of a FAM-N pulse (or indeed the FAM-II pulses on which they are based) depends primarily upon C_Q and the available rf field strength. It was also demonstrated that variation of the asymmetry parameter, η_Q, had a much less significant effect of the form of the optimum FAM-N pulse or on its efficiency. Fig. 2 plots the maximum amount of CT single-quantum coherence obtained in simulation from unit amount of symmetrical triple-quantum coherence as a function of C_Q and ν_1 for spin I=3/2, 5/2, 7/2 and 9/2 nuclei. Note that for each set of C_Q and ν_1 values the maximum efficiency of the optimum FAM-N conversion pulse is plotted (*i.e.*, the exact form of the FAM-N pulses used will vary throughout the plot). To enable direct comparison between results for different spin quantum numbers, simulations have been performed for an identical range of ν_Q^{PAS} (=$3C_Q/4I(2I-1)$ in Hz) [2,3], resulting in different ranges of C_Q values for different I. In all cases, the value of η_Q was fixed at 0. It can be noted that the plots for the conventional, or single-pulse, conversion are consistent with those of Amoureux *et al.* [13] in previous work. For all spins the transfer efficiency increases as ν_1 increases, and as C_Q decreases. (Note that a decrease in efficiency is expected as C_Q tends to 0). The efficiency is effectively constant for a fixed ν_Q^{PAS}/ν_1 (or C_Q/ν_1) ratio. In general, similar observations are found for FAM-N conversion pulses, with efficiency ultimately dropping as C_Q increases. However, it is striking that there appears to be a set of conditions for which FAM-N pulses are most efficient, forming a "band" of high signal intensity in the contour plots in Fig. 2b, d, f and h. Optimum efficiency appears to be achieved when $\nu_1 \approx \nu_Q/6$. The small variation in the simulated efficiency within this region can be attributed, at least partially, to computational accuracy, as the exact FAM-N pulses obtained depend, to some extent, on the number of points and tolerance conditions chosen for the FAM-N optimisations. In the regions of the plot corresponding to low C_Q and high ν_1 the FAM-N efficiency is almost constant, with 0.4–0.5 units of CT coherence created. In this regime, the effect of the FAM-N pulse is similar to a saturation of the transitions, while for the region of higher signal intensity described above, the FAM-N pulse is closer to an inversion (for the majority of crystallites). Under conditions of high C_Q and low ν_1, the efficiency of the FAM-N pulse drops rapidly, although not as severely as that of the single-pulse conversion.

It is clear from Fig. 2 that highest triple-quantum to single-quantum conversion efficiency is not necessarily achieved with the highest rf field available for FAM-N. For example, for ^{87}Rb (I=3/2) with C_Q=1 MHz, η_Q=0, ν_R=12.5 kHz and ν_1=100 kHz, 0.669 units of CT coherence are created by an optimised FAM-N pulse. This drops to 0.571 when ν_1=30 kHz, but also drops (to 0.597) when ν_1=300 kHz. For information on the full density matrices see the Supporting Information. However, for most spin I=3/2 nuclei studied at moderate B_0 field strengths, experimentally available ν_1 values are typically 30–150 kHz and C_Q values vary from 0 to 5 MHz. As a result, experimental conditions are such that the strongest rf field available will generally result in the greatest efficiency for FAM-N pulses. Fig. 2 also shows that the amount of CT coherence created after a FAM-N conversion pulse slightly decreases as I increases. This can be attributed to the creation of additional multiple-quantum coherences, *e.g.*, symmetrical five-quantum coherence for spins I > 3/2). This can be easily seen by considering the evolution of all density matrix elements, as discussed in the Supporting Information. As I increases, the number of possible coherences that may be created by a pulse is increased, reducing the amount of desired symmetrical triple-quantum coherences obtained. A consideration of the full density matrix also explains why FAM-N has a high efficiency at low ν_1 for spin I=3/2 nuclei, but not for higher spin systems. Essentially FAM-N can be considered as a ST-selective pulse, which fundamentally has a different effect for I=3/2 nuclei where only one set ($m_I = \pm 3/2 \leftrightarrow m_I = \pm 1/2$) of STs exist, whereas, for high spins, overlapping signals from multiple pairs of STs will be present. This means that a modulated pulse cannot be perfectly selective for the inner ST when I > 3/2, resulting in unwanted coherence transfer to, for example, five-quantum coherences. As longer modulated pulse trains produce undesired coherence transfer, the FAM-N optimisation pro-

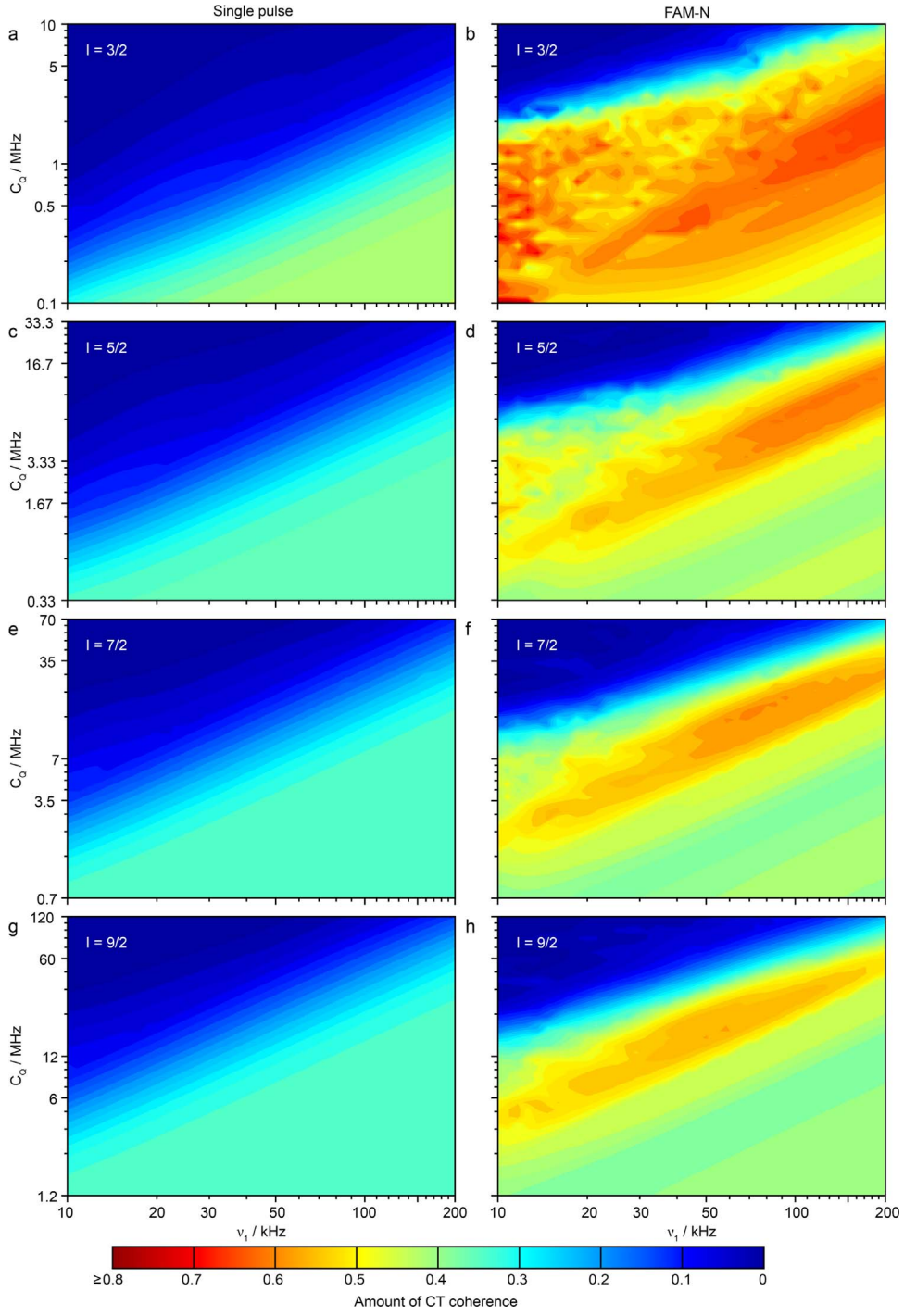

Fig. 2. Log-log contour plots showing the maximum amount of simulated CT single-quantum coherence created after (a, c, e, g) a conventional (single) and (b, d, f, h) FAM-N conversion pulse for a range of C_Q and ν_1 for spin (a, b) I=3/2, (c, d) I=5/2, (e, f) I=7/2 and (g, h) I=9/2 nuclei. The contour levels are set to be identical in all plots to allow a direct comparison. All simulations have been performed for ν_0=196.4 MHz and ν_R=12.5 kHz. C_Q values have been chosen such that the range of ν_Q is the same for the different spins.

cedure generally results in a relatively low number of pulses when I > 3/2. However, for I=3/2 nuclei the modulated pulses only affect the single set of STs and much longer pulse trains produce more efficient conversion in simulation. It should be noted that, experimentally, these longer pulse trains may be subject to more relaxation processes, resulting not only in reduced performance but also in more significant discrepancies between experiment and simulation (see later).

3.2. Effect of MAS rate

It was previously established by Amoureux *et al.* [13] that, unlike the triple-quantum excitation pulse, the conversion pulse in MQMAS experiments is relatively unaffected by the MAS rate, presumably as a result of its shorter duration. This is confirmed in Fig. 3a, where the efficiency of both multiple-quantum excitation (0 to −3Q) and conversion (−3Q to −1Q) is plotted as a function of the MAS rate, simulated for ^{87}Rb (I=3/2) with ν_0=196.4 MHz, ν_1=100 kHz, C_Q=2 MHz and η_Q=0. For excitation, for each value of ν_R the value plotted corresponds to the maximum efficiency of triple-quantum excitation possible (*i.e.*, the duration of the optimum pulse may vary). For conversion, the maximum efficiency for both single pulse (and, subsequently, for FAM-N pulses) was determined from FAM-N optimisations at each of the

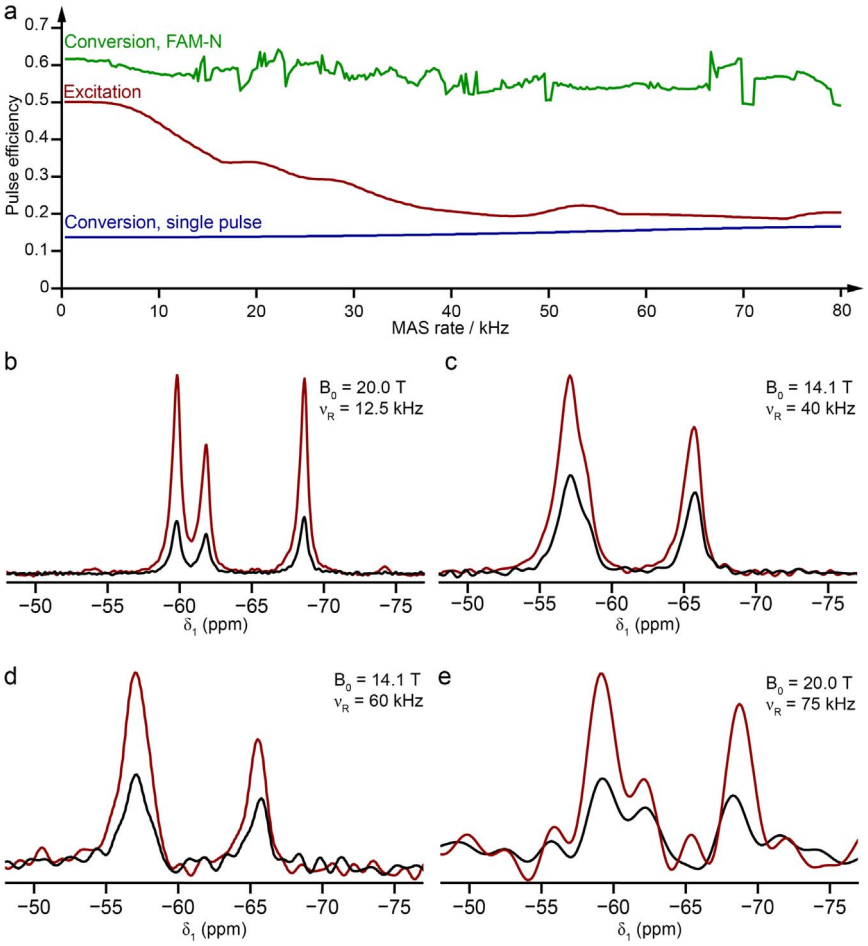

Fig. 3. (a) Simulations of the maximum efficiency of excitation (0 to −3Q, red line), single pulse (−3Q to −1Q, blue line) and FAM-N conversion (−3Q to −1Q, green line) in MQMAS experiments as a function of the MAS rate, ν_R, for ^{87}Rb with B_0=14.1 T (ν_0=196.4 MHz), ν_1=100 kHz, C_Q=2.0 MHz and η_Q=0. For each MAS rate, the excitation pulse was reoptimised, while for the values for single-pulse and FAM-N conversion were determined from FAM-N optimisation for each ν_R. (b-e) Projections of the indirect dimension of ^{87}Rb split-t_1 shifted-echo triple-quantum MAS NMR spectra of $RbNO_3$ recorded with single- (black lines) and FAM-N (red lines) conversion pulses for different MAS rates, ν_R, of (b) 12.5 kHz, (c) 40 kHz, (d) 60 kHz and (e) 75 kHz. Spectra were recorded at (b, e) 20.0 T and (c, d) 14.1 T. (For interpretation of the references to color in this figure legend, the reader is referred to the web version of this article.)

MAS rates. Fig. 3a confirms that the excitation pulse decreases in efficiency as the MAS rate increases, while the conversion pulse remains relatively unaffected. The efficiency of the FAM-N conversion pulse (also plotted in Fig. 3a, green line) also remains relatively constant with respect to the MAS rate. This might seem a little unexpected, given its typically longer duration, but as the optimisation process takes into account the sample spinning the pulse trains that result appear to compensate, at least to some extent, for this effect. The less smooth variation in this plot reflects the changes in the number and duration of pulses used in the FAM-N train, most likely as a result of the small numerical instability in the simulation (and the trade-off between cost and accuracy used in the optimisation procedure) and the similar efficiency of a number of related, but not identical, FAM-N pulses in any one case. When the optimum FAM-N pulses are examined there are some small differences in the pulse trains produced, with generally shorter pulses found for the higher MAS rates.

Fig. 3b–e shows the effect of the experimental application of FAM-N conversion pulses at different MAS rates in ^{87}Rb MQMAS NMR of $RbNO_3$. Projections from the indirect dimension of triple-quantum split-t_1 shift-echo MQMAS spectra are shown. (Note that the B_0 field, and also the appearance/resolution of the spectra, vary.) For faster MAS rates, the smaller rotor size restricts the signal-to-noise ratio and spectra were acquired with lower resolution (*i.e.*, fewer increments) in order to reduce overall experimental times. As seen in the simulations in Fig. 3a, there is not a significant change in the improvement provided by FAM-N pulses at differing spinning speeds, although the best improvement is obtained at the lower MAS rates. Given the variability of experimental parameters with differing spectrometers (and even between experiments carried out on the same spectrometer on different probes), the FAM-N enhancement appears reasonably constant at high MAS rates. Although this experimental parameter is user controlled and can be specified directly within the optimisation, it should be noted that if a FAM-N pulse is optimised at one MAS rate, but applied at a significantly different rate, differences in efficiency may well be observed.

3.3. Effect of offset

The FAM-N optimisations are typically performed assuming that the frequency offset of the applied rf field relative to the isotropic chemical shift of a resonance is 0 (although this parameter could be included in the optimisation procedure if required). However, for samples with multiple sites with differing chemical shifts, each species cannot be placed on resonance simultaneously. Fig. 4 shows the efficiency of a FAM-N pulse optimised with no additional offset, but then applied at offset frequencies varying from +100 to −100 kHz. It can be seen that there is a greater variation in efficiency for FAM-N than for single-pulse conversion, but that FAM-N provides an increase over the conventional pulse over the range of offsets considered (*i.e.*, from ± 100 kHz), ensuring that an advantage will be observed for most

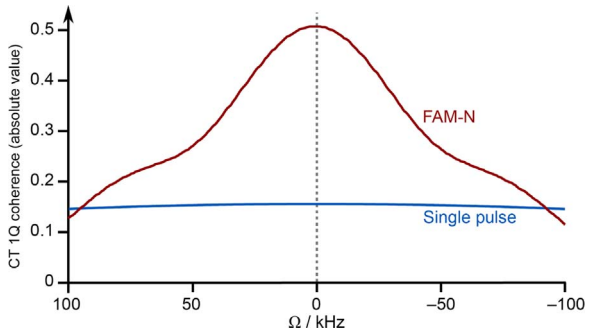

Fig. 4. Plot of the variation in the amount of (absolute value) CT coherence generated from unit triple-quantum coherence of the same sign, by a single or FAM-N conversion pulse. The FAM-N pulse was generated for ^{87}Rb with B_0=14.1 T (ν_0=196.4 MHz), ν_1=100 kHz, ν_R=12.5 kHz, C_Q=2.0 MHz, η_Q=0 and Ω=0.

practically relevant cases. It should be noted that (although not easily seen on Fig. 4 itself) the maximum signal intensity is not obtained for the case of Ω=0, but at a slightly more positive value, reflecting the presence of an isotropic component for the second-order quadrupolar interaction. For the CT this has a powder averaged value of $\nu_{QIS}=((\nu_Q^{PAS})^2/\nu_0)\ A^o(I, m_I)\ (1+\eta_Q^2/3)$, where $A^o(I, m_I)$ are spin- and transition-dependent coefficients (for the $+m_I \leftrightarrow -m_I$ transition) that can be found in the literature [7]). For the system simulated here, ν_{QIS} for the CT is −509 Hz. However, the maximum signal intensity in Fig. 4 is observed at a positive, not a negative, offset. This appears to correspond not to the isotropic shift of the CT, and also not to that for the (unobserved) triple-quantum spectrum (where $A^o(3/2, 3/2)=-3\ A^o(3/2, 1/2)=+1527$ Hz), but is somewhere in between. This probably reflects the dependence of the FAM-N pulses on both CT and 3Q offsets. Similar types of effects have been seen for spin-locking of quadrupolar nuclei [49].

3.4. Applications and limitations

In order to investigate the experimental robustness of the FAM-N approach (*e.g.*, to samples with multiple different sites with differing C_Q values and/or to nuclei with higher spin quantum number) FAM-N conversion pulses were implemented in split-t_1 shifted echo MQMAS NMR experiments for ^{23}Na (I=3/2) NMR of $Na_4P_2O_7$, ^{27}Al (I=5/2) NMR of kyanite (Al_2SiO_5), ^{45}Sc (I=7/2) NMR of Sc_2O_3 and ^{93}Nb (I=9/2) NMR of a 1:1 mixture of $LiNbO_3$ and $NaNbO_3$. Projections of the indirect dimension of the MQMAS spectra are shown in Fig. 5a, c, e and g, respectively. In each case, the duration of the single pulse was optimised experimentally, while the FAM-N pulse was used without any experimental reoptimisation. For the FAM-N optimisations, accurate values of the rf field strength (as measured on a sample with C_Q=0) and MAS rate were used. In some cases, the C_Q and η_Q values chosen for the optimisation were those for one of the sites in the sample (known from the literature) while, in others, an "average" or "intermediate" value was chosen (as described below). Fig. 5b, d, f and h show simulations of the efficiency of both single and FAM-N conversion pulses used in the experiments as a function of C_Q [37]. The C_Q value used for the FAM-N optimisation is indicated by a solid black line, and the C_Q values for each of the sites in the sample are shown by dashed lines. Note that the plots do not consider any variation in η_Q, and this may lead to some small differences between experimental efficiencies and simulations. In all simulations, the effect of the excitation pulse was not taken into account, but this will have an impact on the absolute and relative intensities observed in experimental spectra [13]. However, the relative signal intensities observed for spectra recorded with single and FAM-N conversion pulses (given in Table 1 for both experiment and simulation) is not affected by the efficiency of the excitation pulse.

For $Na_4P_2O_7$, there are four distinct Na sites, each of which have similar C_Q values (shown in Fig. 5b), which can be resolved easily using MQMAS and have been assigned only relatively recently using NMR crystallography [50,51]. The FAM-N pulse used experimentally was produced using C_Q=2.0 MHz (and η_Q =0) in the optimisation. All four Na species are well resolved in the MQMAS spectrum (shown in Fig. 5a), and exhibit a very similar enhancement (of a factor of ~2) when FAM-N conversion is used. Fig. 5b shows that while the single-pulse conversion efficiency decreases steadily as C_Q increases (over the range considered) the FAM-N efficiency (although consistently much higher) does show some variation, but is most efficient at the value for which it was optimised. The relative intensity of the resonances observed experimentally (Na1 > Na3 > Na2≈Na4) when FAM-N is used is consistent with that predicted by simulation (with the small relative differences probably due to the different efficiencies in the excitation pulse). The enhancements using FAM-N observed experimentally appear smaller than those predicted theoretically in all cases (Table 1). However, in each case, Na2 shows the lowest enhancement, and Na3/Na1 the highest enhancements. As described above, the application of FAM-N to I=3/2 systems is fundamentally different from its use for systems with higher spin quantum number, where other symmetrical multiple-quantum coherences are present, more than one type of ST exists, and the pulses produced are typically longer (both in the total number of pulses and the total duration of the pulse train). This latter point may provide a possible explanation for the enhancement differences observed between experiment and theory, as it might be expected that relaxation processes may play a more significant role. Table 1 also shows that the discrepancy between theory and experiment is greater for this sample than for the results obtained for higher spin systems. Additional explanations for the discrepancy observed here will be considered in more detail in a later section.

Among the commonly-studied quadrupolar nuclei, ^{27}Al has one of the largest ranges of ν_Q observed for typical samples [1–3]. Kyanite, a silicate mineral typically found in metamorphic and sedimentary rocks, is one of the polymorphs of Al_2SiO_5, and has four distinct Al sites (with C_Q values ranging from ~4 to ~10 MHz), which are known to be difficult to resolve (and indeed to assign) by MQMAS at moderate field owing to the similarity of the Al1 and Al4 species, but have been resolved in experiments with higher sensitivity (*i.e.*, those enabling higher resolution without a significant signal-to-noise penalty) including CPMG-MQMAS and STMAS [52,53]. The FAM-N pulse used for this challenging sample was optimised with C_Q=6.0 MHz and η_Q=0 (*i.e.*, an "average" C_Q value). Although the absolute intensities observed experimentally again differ from those predicted by simulation (for the reasons discussed above), the relative efficiency of experiments carried out using FAM-N are similar between Fig. 5b and d. Simulations show that FAM-N conversion is most efficient for the site with parameters closest to those used in the optimisation, although good efficiency is observed over the wide range of C_Q values considered. The poor efficiency of the single-pulse conversion at higher C_Q values (but the good efficiency of FAM-N at these values) results in similar enhancements for Al1/Al4 and also for Al3 where the pulse is most efficient. Good sensitivity is seen for Al2 (with the lowest C_Q value) but the enhancement is poorer owing to the increased efficiency of single-pulse conversion. Overall, and unlike $Na_4P_2O_7$, the magnitude of the improvement predicted by simulation is reflected in experiment. Furthermore, the much larger range of C_Q values present ensure that the effect of neglecting other factors, *e.g.*, η_Q or Ω, is less significant.

Fig. 5c shows the ^{45}Sc isotropic MQMAS spectrum of Sc_2O_3, which contains two distinct Sc sites with very different C_Q values (~15.3 MHz and ~23.4 MHz) [54]. Given the large difference in C_Q, and the poor efficiency of single-pulse conversion at higher C_Q values, the FAM-N pulse was optimised with C_Q=23.4 MHz. The enhancement obtained experimentally using FAM-N is of similar magnitude to that predicted in the simulation, although the enhancement seen for Sc2 is greater experimentally than that predicted (and seems to be better than that

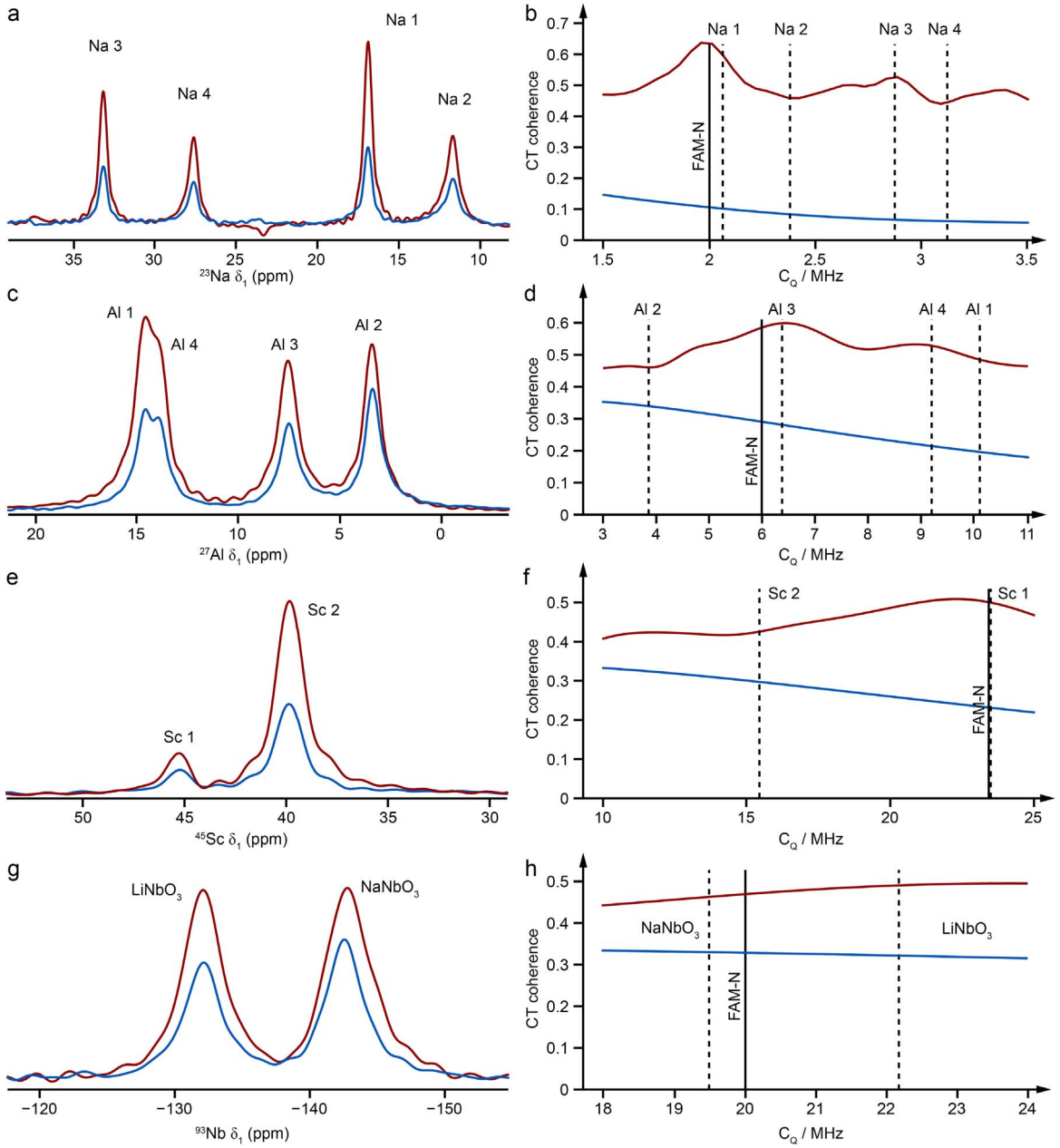

Fig. 5. (a, c, e, g) Projections of the indirect dimension of split-t_1 shifted-echo triple-quantum MAS NMR spectra, recorded with a single (blue line) and FAM-N (red line) conversion pulse for (a) ^{23}Na (I=3/2) NMR of $Na_4P_2O_7$, (c) ^{27}Al (I=5/2) NMR of kyanite (Al_2SiO_5), (e) ^{45}Sc (I=7/2) NMR of Sc_2O_3 and (g) ^{93}Nb (I=9/2) of a 1:1 M mixture of $LiNbO_3$ and $NaNbO_3$. For more detailed experimental parameters see the Supporting Information. (b, d, f, h) Numerical simulation of the amount of CT single-quantum coherence, generated from initial unit 3Q coherence using a single (blue line) and FAM-N (red line) conversion pulse as a function of C_Q (assuming η_Q=0). The C_Q value used for the FAM-N optimisation is indicated by a solid black line, and the C_Q values for each of the sites in the sample are shown by dashed lines. (For interpretation of the references to color in this figure legend, the reader is referred to the web version of this article.)

obtained for Sc1). It should be noted that, although simulated for a system with C_Q=23.4 MHz, the FAM-N pulse produced is predicted to have an optimum efficiency at a slightly lower C_Q value (~22 MHz). It may be that this difference results from the large η_Q for Sc2 (0.62), the effect of which is not included in the simulation in Fig. 5f. If the efficiency of the FAM-N pulse used is simulated for a site where C_Q=23.4 MHz and η_Q=0.62, the enhancement predicted increases from ×1.4 (Fig. 5f and Table 1) to ×1.6, which is indeed closer to experiment. It should also be noted that the larger the values of C_Q used in the FAM-N optimisation, the longer pulse trains tend to be produced, which can also can result in small differences between experiment and theory.

^{93}Nb is a spin I=9/2 nucleus, with high natural abundance and high γ. For relatively symmetrical (*i.e.*, NbO_6) environments C_Q values are sufficiently small that MAS (and, therefore, MQMAS/STMAS) experiments are feasible at moderate B_0 and moderate ν_R [47,55,56]. $LiNbO_3$ and $NaNbO_3$, which adopt perovskite (or perovskite-type) structures, have a single Nb site with similar C_Q, but different values of η_Q (0.2 for $LiNbO_3$ and 0.8 for $NaNbO_3$) [47,55]. It has been shown that samples of $NaNbO_3$ can contain more than one room-temperature polymorph (*i.e.*, both *Pbcm* and $P2_1ma$ polymorphs often co-exist, depending on the synthesis route), although all have very similar ^{93}Nb NMR parameters [55,56]. Therefore, the C_Q value shown on Fig. 5h was obtained from a fit of the ^{93}Nb MAS spectrum of the $NaNbO_3$ sample used in this work (with C_Q=19.5 MHz and η_Q=0.8). The FAM-N pulse was optimised for C_Q=20 MHz and η_Q=0.0. Under the conditions specified the optimum FAM-N pulse produced is composed of only two pulses, and results in relatively low enhancements both theoreti-

Table 1
Theoretical (assuming no variation in η_Q) and experimental signal enhancements found when using FAM-N pulses compared with a single pulse for the conversion of triple-quantum coherences to CT coherence of the same sign for the systems in Fig. 5. Details of the FAM-N pulses used can be found in the Supporting Information.

Sample	Species	Enhancement	
		Theoretical	Experimental
$Na_4P_2O_7$	Na1	×3.4	×2.4
	Na2	×3.1	×1.9
	Na3	×4.4	×2.3
	Na4	×4.4	×2.1
Al_2SiO_5	Al1	×1.4	×1.4
	Al2	×1.9	×1.7
	Al3	×2.0	×2.0
	Al4	×2.0	×1.7
Sc_2O_3	Sc1	×2.1	×1.7
	Sc2	×1.4	×2.1
$LiNbO_3/NaNbO_3$	$LiNbO_3$	×1.5	×1.6
	$NaNbO_3$	×1.4	×1.4

cally and experimentally. As shown in Fig. 5h, the FAM-N efficiency is predicted to be very similar for both C_Q values. However, the steady decrease in efficiency of the single pulse conversion results in a slightly better enhancement for $LiNbO_3$, a prediction that is reflected experimentally (as shown in Fig. 5g). The magnitude of the enhancement obtained experimentally is in good agreement with that predicted in simulation, and this remains the case even when η_Q is included in the simulation (with changes in the enhancements of only 1–3%).

3.5. Applications to more challenging systems

The experiments discussed above, and those shown in previous work [37] confirm that FAM-N pulses produce a significant improvement in the ±3 to ±1 conversion efficiency for a wide range of materials, for nuclei with differing spin quantum number and varying C_Q values, with no experimental optimisation, even when exact NMR parameters are not known. These properties make FAM-N particularly attractive for use on more challenging samples, *i.e.*, with very poor sensitivity, where experimental optimisation of a complex composite pulse is usually not possible. Poor sensitivity may result for species with low γ, low natural abundance, or large quadrupolar interactions (or indeed from combinations of these). It is for these "real" samples that FAM-N should prove invaluable in improving sensitivity, or perhaps even just to enable a spectrum to be recorded. Fig. 6 shows four examples of the application of FAM-N to challenging samples, with the theoretical and experimental enhancements in each case given in Table 2.

Fig. 6a shows isotropic projections of ^{71}Ga MQMAS spectra (acquired at a MAS rate of 33.3 kHz using single pulse and FAM-N conversions) of $GaPO_4$ (berlinite), which exhibits a single ^{71}Ga site with a C_Q of 8.8 MHz [57]. At moderate field (*i.e.*, 14.1 T, in house) this is towards the upper limit of ν_Q^{PAS} values (~2.2 MHz) that it is feasible to consider for MAS and MQMAS experiments. As C_Q values and, therefore, second-order quadrupolar broadening increase, faster MAS rates are required to obtain powder lineshapes that are well separated from spinning sidebands. At 14.1 T, the ^{71}Ga CT MAS lineshape for berlinite is ~27 kHz in width, necessitating MAS rates above this to be used. The use of fast MAS, however, poses additional limits on sensitivity, owing to the smaller rotors used, even if experiments are equally efficient as the spinning speed increases. Fig. 3 showed that the efficiency of FAM-N remains reasonably constant at high MAS rate, suggesting it is an appropriate method for increasing sensitivity for species with high C_Q subject to rapid MAS. Fig. 6a shows an experimental enhancement of a factor of 3, in reasonably good agreement with that predicted theoretically (3.3), although, as above, the longer pulse trains that result for spin I=3/2 nuclei, probably contribute to any differences. The poor sensitivity for this sample is clear, despite the long acquisition time (~52 h). The large C_Q value does result in significant lineshape distortions in MQMAS experiments (owing to the non-uniform triple-quantum excitation and conversion with respect to crystallite orientation), making it extremely challenging to fit the quadrupolar lineshape. The centre of gravity of the lineshape can be easily determined from the FAM-N MQMAS spectrum, giving P_Q=9.2 MHz, in good agreement with the literature [57,58].

Projections of ^{27}Al MQMAS spectra of the andalusite polymorph of Al_2SiO_5, acquired using single pulse and FAM-N conversion pulses, are shown in Fig. 6b. Andalusite has two ^{27}Al sites, with C_Q values of 5.6 and 15.3 MHz, labelled here as Al1 and Al2, respectively [59], posing a significant sensitivity challenge for conventional MQMAS. Furthermore, the very large C_Q (ν_Q^{PAS}=1.15 MHz) and spin quantum number result in the presence of a third-order splitting in STMAS spectra, limiting resolution [15,60]. Although this can be removed by a modification of the STMAS experiment (SCAM-STMAS) [15,61], the additional pulses required do decrease sensitivity, and MQMAS experiments (which are unaffected by this interaction) remain a useful alternative if sensitivity can be improved. The FAM-N pulse used in Fig. 6b was optimised for the site with the largest C_Q value (Al2), and shows an experimental enhancement of ×1.3 for Al1 and ×2.2 for Al2, in good agreement with the values predicted theoretically (and given in Table 2). The poor sensitivity of conventional MQMAS is clear, with the signal for Al2 just above the level of the noise, and NMR parameters cannot be easily extracted. In contrast, the sensitivity advantage of FAM-N conversion enables the centre of gravity of the lineshapes to be easily determined and NMR parameters to be extracted that are in good agreement with previous literature [59].

Brucite is the mineral form of $Mg(OH)_2$ and contains a single distinct ^{25}Mg species, with C_Q=3.1 MHz and η_Q=0 [44]. ^{25}Mg NMR can be challenging, as this isotope has a natural abundance of 10%, a low γ and typically large quadrupolar broadening (partially as a consequence of the low γ). Furthermore, the low γ also restricts the available B_1 fields, reducing the efficiency of triple-quantum filtration. However, ^{25}Mg STMAS spectra of brucite have been obtained for both enriched (99%) and natural-abundance samples, in 6 and 66 h, respectively [62]. Both spectra showed evidence for a third-order splitting, suggesting efficient MQMAS experiments may provide a desirable alternative. As only a single ^{25}Mg species is present for brucite, the enhancement provided by FAM-N conversion pulses can be measured simply by a triple-quantum filtered experiment, as shown in Fig. 6c, rather than a time-consuming complete two-dimensional experiment. In order to improve overall sensitivity, experiments have been carried out at 20.0 T. Despite the poor sensitivity, the enhancement obtained experimentally using FAM-N (see Table 2) is ×3.3 (lower than the theoretical prediction of ×4.8). Although there is an overall improvement in sensitivity, there does seem to be a significant lineshape distortion observed in the FAM-N experiment, (although it should again be noted that the conventional MQMAS experiment also produces lineshape distortions, particularly at low rf). This distortion is also reproduced in simulation (see the Supporting Information), showing it results from FAM-N conversion rather than other experimental imperfections. It is possible to estimate the "amount of distortion" of a given lineshape by defining it as the standard deviation of $\langle I^{CT} \rangle$ for the different crystallite orientations. For brucite, a single pulse conversion gives a deviation in the magnitude of $\langle I^{CT} \rangle$ of 38% (0.119 ± 0.045) and a phase distortion of ± 7.4°, while FAM-N conversion results in 41% (0.534 ± 0.218) and ± 16.2°. Although FAM-N conversion produces a more significant variation in the amplitude, this is very similar to the single pulse conversion when expressed as a % of the total magnitude. There is a slight increase in the phase variation when FAM-N is used. In general, no significant difference in the "amount" of lineshape distortion

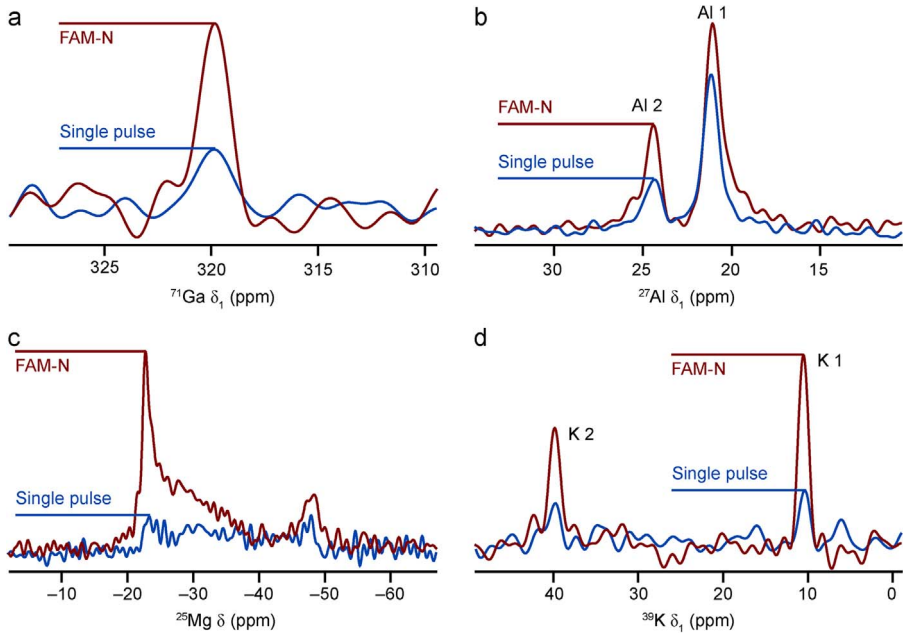

Fig. 6. (a, b, d) Projections of the indirect dimension of split-t_1 shifted-echo triple-quantum MAS NMR spectra, and (c) triple-quantum filtered MAS NMR spectrum recorded with a single or FAM-N conversion pulse for (a) ^{71}Ga (I=3/2) NMR of $GaPO_4$ (berlinite), acquired in 52 h at 14.1 T, (b) ^{27}Al (I=5/2) NMR Al_2SiO_5 (andalusite), acquired in 11 h at 14.1 T, (c) ^{25}Mg (I=5/2) NMR of $Mg(OH)_2$, acquired in 27 h at 20.0 T and (d) ^{39}K (I=5/2) NMR of K_2SO_4, acquired in 32 h at 18.8 T. For more detailed experimental parameters see the Supporting Information.

Table 2
Theoretical and experimental signal enhancements found when using FAM-N pulses compared with a single pulse for the conversion of triple-quantum coherences to CT coherence of the same sign for the systems in Figs. 6 and 7. Details of the FAM-N pulses used can be found in the Supporting Information.

Sample	Species	Enhancement	
		Theoretical	Experimental
$GaPO_4$ (berlinite)	Ga1	×3.3	×3.0
Al_2SiO_5 (andalusite)	Al1	×1.4	×1.3
	Al2	×2.1	×2.2
$Mg(OH)_2$ (brucite)	Mg1	×4.8	×3.3
K_2SO_4	K1	×4.0	×3.6
	K2	×3.5	×3.0
α-Mg_2SiO_4 (forsterite)	Mg1	×2.4	
	Mg2	×2.0	×1.9

produced by FAM-N is expected, but the distortions observed are different (*i.e.*, different crystallite orientations are underrepresented in the two different spectra). Although the enhancement observed is slightly lower than that predicted theoretically, it is significant (giving a time saving of a factor of ~11) and was achieved without any experimental reoptimisation of the FAM-N pulse, emphasising the applicability of this approach to systems with low sensitivity where experimental optimisation is not possible.

Approximately 85% of NMR-active nuclei have γ lower than that of ^{13}C. This includes ^{39}K, where the low γ not only limits sensitivity, but also increases the magnitude of the second-order quadrupolar broadening and restricts the available rf field strength, as discussed for ^{25}Mg above. However, in contrast to ^{25}Mg, ^{39}K has a 93% natural abundance, and typically exhibits low C_Q values (~0–1.5 MHz) and so is usually an easier nucleus to observe. Fig. 6d shows the isotropic projections of ^{39}K triple-quantum MAS NMR spectra of K_2SO_4, recorded using a single pulse and a FAM-N pulse for multiple-quantum conversion. This material possesses two distinct ^{39}K species, with δ_{iso}=−6 ppm, C_Q=0.95 MHz, η_Q=0.05 (labelled K1) and δ_{iso}=6 ppm, C_Q=0.85 MHz, η_Q=0.95 (labelled K2) [62,63]. Note the labels used here do not refer to crystallographic species. In previous work, high-resolution spectra were obtained using STMAS, but the authors were unable to obtain MQMAS spectra at the field used (9.4 T) [62]. The spectra in this work were acquired at 18.8 T, and the FAM-N pulse was optimised using C_Q=0.9 MHz and η_Q=0. The enhancements observed experimentally (×3.6 and ×3.0) are in good agreement with those predicted theoretically (×4.0 and ×3.5). This confirms the observation in Fig. 2 that FAM-N enhancements are expected to be higher when low rf field strengths are used, and is one of a few cases for I=3/2 nuclei where the simulation accurately predicts the magnitude of the signal enhancement. The sensitivity obtained at 18.8 T in 32 h not only enables both sites to be resolved, but also for cross sections to be extracted and fitted to obtain accurate quadrupolar parameters for both sites.

Forsterite (α-Mg_2SiO_4) is the Fe-free end member of the olivine solid solution, and as $Mg_{1.8}Fe_{0.2}SiO_4$, is the principal component of the Earth's upper mantle. As such, this has led to significant interest in its study using NMR spectroscopy and supporting first-principles calculations, which are summarised in Ref. [64]. Although extensive ^{17}O and ^{29}Si NMR studies exist, relatively few ^{25}Mg investigations have been undertaken, owing to the less favourable properties of this nuclide, discussed above. The ^{25}Mg quadrupolar parameters were initially measured using single-crystal NMR spectroscopy [65] and the values determined supported by first-principles calculations [64,66]. Forsterite contains two distinct Mg species (Mg1 with C_Q=5.3 and η_Q=0.99 and Mg2 with C_Q=4.4 and η_Q=0.4), which appear overlapped in the MAS spectra at moderate to high fields, requiring high-resolution methods to be employed. However, the high C_Q values, and low rf fields, pose a significant experimental challenge. Although Davis *et al.* were able to obtain a (natural abundance) ^{25}Mg MQMAS spectrum [67], this experiment was carried out at 19.5 T, using a probe optimised to produce high rf field strengths at low frequencies and employed SPAM pulses for sensitivity enhancement.

Fig. 7a shows MAS and CPMG-MAS NMR spectra (shown both as spikelets and as summed echoes) of forsterite, acquired at 18.8 T. The two lineshapes are overlapped at this field strength, although their contributions to the CPMG-MAS lineshape are simulated in Fig. 7b.

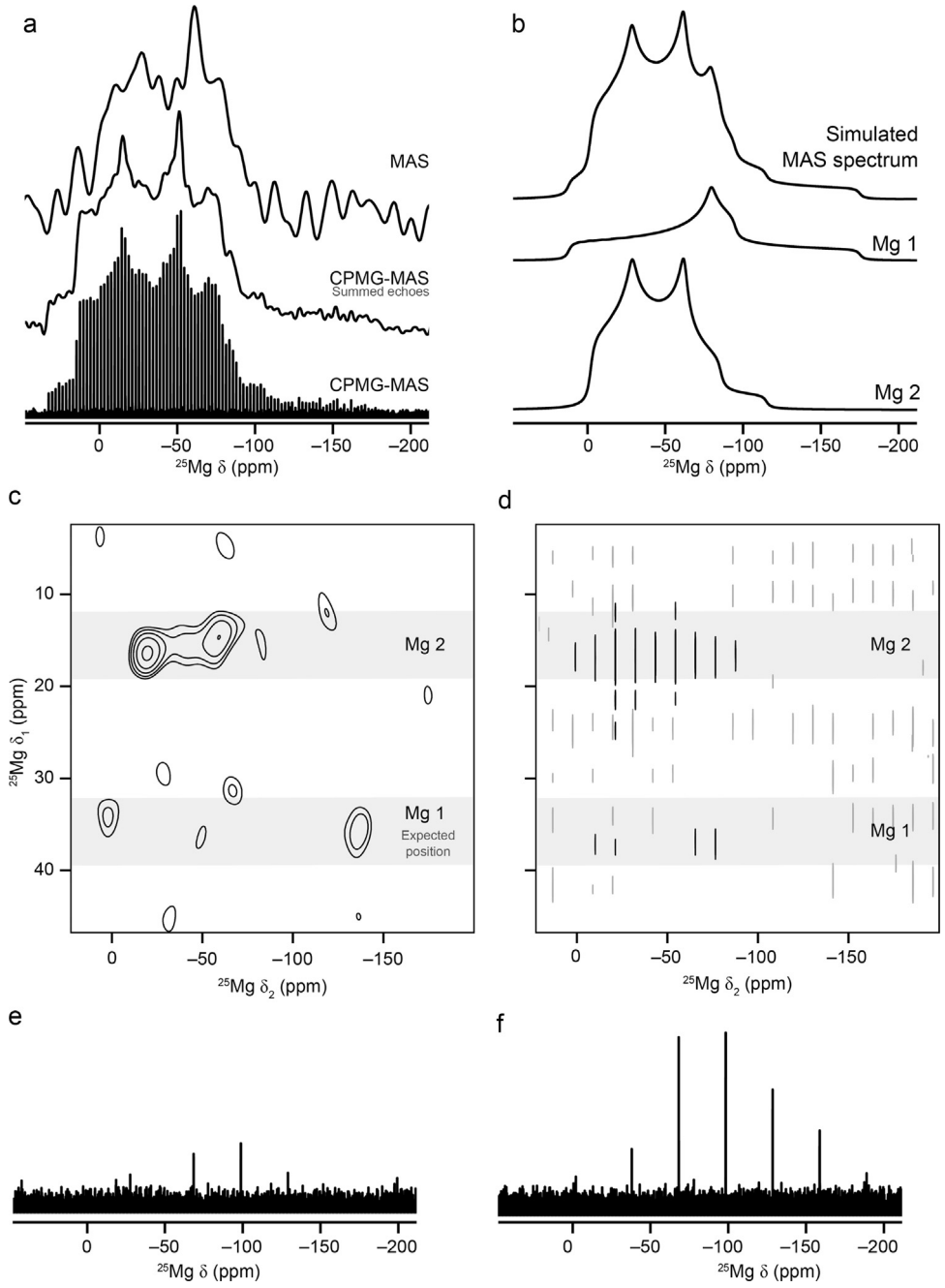

Fig. 7. (a) Experimental ^{25}Mg MAS, CPMG-MAS (summed echoes and shown as splikelets) NMR spectra of α-Mg_2SiO_4 (forsterite), acquired at 18.8 T with 14 kHz MAS. (b) Simulation of the contributions of the two Mg species to the CPMG-MAS NMR spectrum of forsterite. (c, d) Two-dimensional ^{25}Mg (20.0 T) split-t_1 shifted echo (c) MQMAS (14 kHz MAS, 48 h) and (d) MQMAS-CPMG (13.33 kHz MAS, 88 h) spectra of α-Mg_2SiO_4, with FAM-N used for conversion of multiple-quantum coherences. (e, f) Triple-quantum filtered ^{25}Mg (14.1 T) MAS-CPMG NMR spectra of α-Mg_2SiO_4 (14.1 T, 13.333 kHz, 38 h) with (e) a single pulse and (f) FAM-N used for conversion of multiple-quantum coherences.

The MAS spectrum (recorded in 9 h) displays poor sensitivity, while the use of CPMG enables a spectrum with much better sensitivity to be acquired in half of the time (5 h). This improvement is a result of the very long T_2 relaxation times (exceeding several hundred ms), enabling multiple echoes to be acquired, and resulting in very narrow spikelets. In order to resolve the two Mg sites, MQMAS is required, and Fig. 7c shows a two-dimensional MQMAS NMR spectrum of forsterite, acquired at 20.0 T, using FAM-N for conversion of multiple-quantum coherences. The lineshape attributed to Mg2 is clear in this spectrum but there is little signal observable for Mg1. This site has both a larger C_Q value (and so less efficient excitation and conversion of multiple-quantum coherences), and a larger η_Q (and so larger P_Q), resulting in a much broader, lower intensity, line that is more difficult to observe when sensitivity is poor. Furthermore, this site appears to exhibit slower T_1 relaxation. This explains the unexpected difference in relative intensities for the two Mg sites in the MAS spectrum (1.9:1 in Fig. 7a, acquired with a recycle interval of 35 s, rather than the 1:1 expected from the crystal structure). Relaxation measurements (using a CPMG saturation-recovery experiment) revealed a T_1 value of ~25 ± 6 s for Mg2, but in excess of 90 s for Mg1. As with MAS spectra MQMAS sensitivity can also be improved using CPMG in acquisition, as described earlier [34], and some signal is now observed for Mg1 (Fig. 7d), enabling the position of the resonance in the isotropic dimension to be determined unambiguously. Although a clear quadrupolar lineshape cannot be extracted, it is possible to extract the position of the centre-of-gravity of the lineshape and estimate a P_Q

value (~6.3 MHz) that is in reasonable agreement with the literature (5.8 MHz), given the sensitivity. It is difficult to measure the enhancement provided by FAM-N from two-dimensional MQMAS spectra given the long acquisition times, but this can be estimated from the triple-quantum CPMG-MAS NMR spectra (acquired at 14.1 T) shown in Fig. 7e and f. The experimental improvement can be estimated to be ×1.9 for Mg2, in good agreement with the theoretical prediction of ×2.0. Although a similar improvement is predicted for Mg1 (×2.4), it is not possible to determine the experimental value from the spectra in Fig. 7e and f. This suggests that a corresponding spectrum to that in Fig. 7d acquired with a single pulse for conversion of multiple-quantum coherences would take 352 h (15 days) to obtain, showing the applicability of FAM-N pulses for use on challenging samples.

3.6. Other effects

We have shown (both here and previously) that considerable sensitivity enhancements can still be obtained with FAM-N pulses when they are applied at conditions that vary from those used in the optimisation process (either because not all relevant information is available in advance or owing to the presence of multiple sites with different NMR parameters). Any differences in the parameters used/found experimentally will inevitably result in experimental enhancements that differ from those predicted theoretically. However, in some cases, the enhancements obtained in experiment show more significant differences to theory than expected. For example, the ^{23}Na MQMAS NMR spectrum of $Na_4P_2O_7$ shown in Fig. 5a exhibits a considerably lower enhancement (by a factor of ~2) upon the inclusion of FAM-N pulses than predicted theoretically. This is not expected to be a particularly challenging system, and although four sites are present their NMR parameters are more similar than many of the systems discussed above.

In order to investigate possible causes for the difference in experimental and theoretical enhancements for ^{23}Na NMR of $Na_4P_2O_7$, the effect of additional parameters on the performance of FAM-N pulses need to be considered. A FAM-N pulse is initially optimised using a set of typical/average ^{23}Na NMR parameters (in this case, B_0=14.1 T, C_Q=2 MHz, η_Q=0.0, ν_1=95.8 kHz, ν_R=12.5 kHz). The optimised pulse train produced is composed of 12 alternating pulses, and has a total duration of 9.59 μs. Maximum conversion efficiency with a single pulse under similar conditions is obtained with a pulse of duration 1.5 μs. The maximum enhancement produced by such a pulse is ×3.3. Table 3 shows the amounts of signal obtained in simulation (and the relative enhancement ratios) when single and optimised FAM-N conversion pulses are applied under a range of different conditions. The theoretical efficiencies of the two conversion pulses for species with C_Q values corresponding to those for the four Na species in $Na_4P_2O_7$ is shown in Table 3 (column headed C_Q). Although now being applied under conditions that vary from those for which the FAM-N pulse was optimised, the predicted enhancement (over a single pulse) from using FAM-N increases (*e.g.*, for Na3 from ×3.3 to ×4.3). This does not reflect any increase in efficiency for FAM-N, which remains the same for Na2 (which has C_Q=2 MHz), and decreases for Na2, Na3 and Na4, but from the decreased efficiency of single pulse conversion as the C_Q value increases. (These efficiencies correspond to those simulated in Fig. 5b).

In reality, the four Na sites do not have η_Q=0 (as used in the FAM-N optimisation), and it might be expected that applying FAM-N to species with higher η_Q will again reduce the efficiency. Table 3 shows this is indeed the case (column headed η_Q) and, as the single pulse efficiency is not affected significantly by a variation in η_Q, the predicted FAM-N enhancement decreases. The four Na species also exhibit differences in their isotropic chemical shifts (from −5.3 to +3.2 ppm). However, Table 3 shows that this produces very little difference in the efficiency of multiple-quantum conversion using single pulses or FAM-N pulses, and only small changes are seen in the enhancement ratios (column headed δ_{iso}). This observation is in agreement with the simulation in Fig. 4, which showed FAM-N pulses had very little offset dependence over the shift range considered here.

Table 3
Amount of simulated ^{23}Na CT coherence generated from unit triple-quantum coherence of the same sign, using either a single pulse or FAM-N conversion pulse, and the corresponding theoretical enhancement ratios, when pulses are applied to the four distinct Na species in $Na_4P_2O_7$. The effect of applying the initial (or ideal) FAM-N pulse at different conditions (including the correct C_Q, η_Q and δ_{iso}) and some estimation of the effects of relaxation and the probe hardware are included.

		Initial[a]	Additionally including					
			C_Q	η_Q	δ_{iso}	T_2 (iso)	Filter	Filter (opt)
Na1	single	0.15	0.14	0.14	0.15	0.15	0.12	0.15
	FAM-N	0.49	0.49	0.43	0.43	0.41	0.33	0.33
	Ratio	×3.3	×3.5	×3.1	×2.9	×2.7	×2.8	×2.2
Na2	single	0.15	0.13	0.14	0.14	0.14	0.11	0.14
	FAM-N	0.49	0.40	0.37	0.36	0.34	0.28	0.28
	Ratio	×3.3	×3.1	×2.6	×2.6	×2.4	×2.5	×2.0
Na3	single	0.15	0.10	0.11	0.11	0.11	0.09	0.11
	FAM-N	0.49	0.43	0.38	0.37	0.36	0.29	0.29
	Ratio	×3.3	×4.3	×3.5	×3.4	×3.3	×3.2	×2.6
Na4	single	0.15	0.09	0.10	0.10	0.10	0.08	0.10
	FAM-N	0.49	0.38	0.34	0.34	0.33	0.26	0.26
	Ratio	×3.3	×4.2	×3.4	×3.4	×3.3	×3.3	×2.6

[a] optimised for B_0=14.1 T (ν_0=158.8 MHz), C_Q=2.0 MHz, η_Q=0.0, ν_1=96 kHz, ν_R=12.5 kHz.

One additional difference between experimental application of FAM-N pulses and theoretical simulations of their efficiency is the possible effects of relaxation. The FAM-N pulse trains are in most cases much longer than the single pulses used for multiple-quantum conversion, and so the effects of relaxation might be considered to be of greater importance. For the case considered here, the two pulse durations are 9.59 and 1.5 μs, respectively. While it is not possible to include relaxation in the theoretical simulations, and it is difficult to measure relaxation (or relaxation differences) between sites in a multi-dimensional experiment, an estimate can be obtained from the Na1-Na4 linewidths in the isotropic dimension of the MQMAS spectra in Fig. 5a (which are affected by evolution under both single- and multiple-quantum coherences). To attempt to account for this, the efficiency of the FAM-N conversion pulse was scaled by exp $(-(\tau_{FAM\text{-}N}-\tau_{single})/T_2(iso))$, where τ is the length of the two types of pulse, as shown in Table 3 (column headed T_2(iso)). Only a small change in efficiency is observed, with the highest loss seen for Na2, which exhibits the broadest line.

The experimental efficiency of all pulses is also reduced by hardware-related factors. Many are difficult or impossible to take into account (*e.g.*, the accurate generation of pulse lengths, the errors in rf calibration or the variation of this quantity across the sample, detuning of the probe during an experiment, *etc.*,), but the effect of the probe itself can be estimated. The probe can be considered as a bandpass RLC circuit, characterised by a resonance frequency (ν_{rf}) and a pass-band width. The effect of an electronic filter on an alternating voltage is described by a transfer function H_F (defined in the frequency domain by U_s/U_e, where U_e and U_s are the voltages applied by the amplifier and observed at the terminals of the RF coil, respectively). Although the typical maximum excitation bandwidth of a conventional NMR probe can be estimated as ~200 kHz, the fast phase changes required by FAM-N are equivalent to a frequency more remote from ν_{rf}, and are, therefore, attenuated. This results in a rise time (*i.e.*, the time required by a voltage from the amplifier to appear at the terminals of the rf coil), which can affect the efficiency of the pulses. It is difficult to determine the related transfer function theoretically, but the rise time can be measured directly using an oscilloscope, and a transfer function

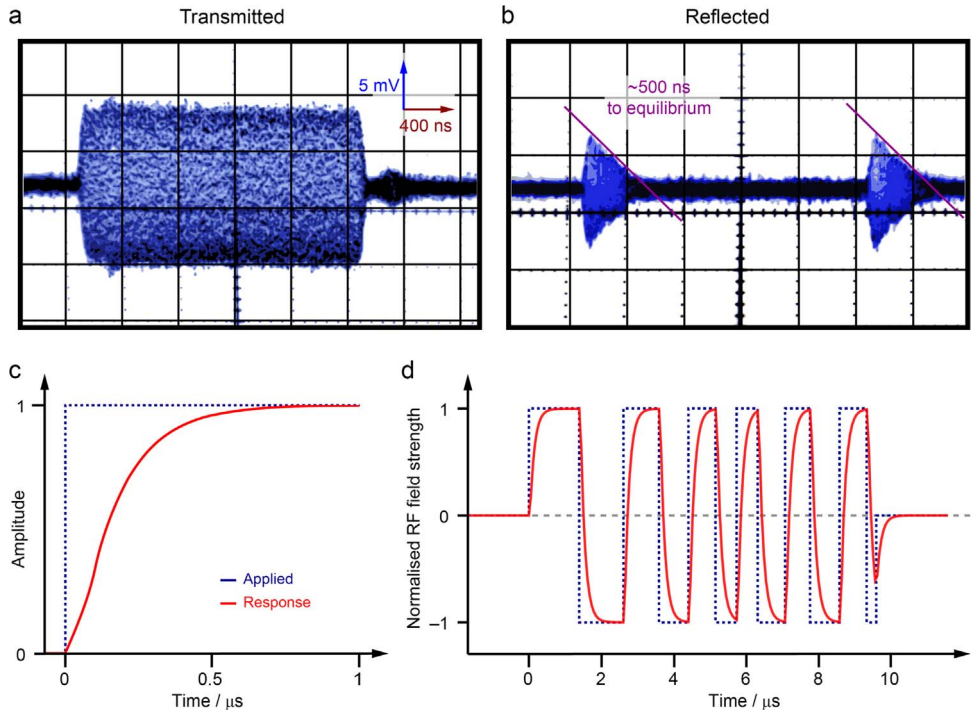

Fig. 8. (a, b) Screen captures of an oscilloscope showing (a) the voltage transmitted to the probe and (b) the voltage reflected by the probe used to acquire the spectra in Fig. 5a, upon application of a pulse with ν_0=158.8 MHz, τ=2 us and power 0.5 W. (c, d) Schematic showing the effect of a filter (transfer function H_F) on (c) a simple step function and (d) the FAM-N pulse used in Fig. 5a.

constructed to reproduce this. Fig. 8a and b shows the transmitted and reflected voltage for the probe used for the experiments on $Na_4P_2O_7$, respectively, as measured on an oscilloscope, showing that the reflected power disappears only after 500 ns from a voltage change. A simple transfer function can be constructed using Matlab ("*fdesign*" command). Rather than using a bandpass filter (centred on ν_{rf}), a lowpass filter with a passband frequency of 200 kHz (passband attenuation 0.1 dB) and a stopband frequency of 8 MHz (stopband attenuation 12 dB) was used. The expected response of the probe (determined from the convolution of the Fourier transform of the transfer function and the applied voltage) is shown in Fig. 8c (and confirms a rise time of 500 ns). The effect of this transfer function on the FAM-N pulse used for ^{23}Na MQMAS NMR of $Na_2P_2O_7$ is shown in Fig. 8d. Using this modified FAM-N pulse in the simulation gives the enhancement ratios shown in Table 3 (column headed filter). Although the filter has a significant effect on the efficiency of the FAM-N pulse (reducing it by ~20%), the efficiency of single pulse conversion of triple-quantum coherences is also reduced, resulting in a very similar enhancement ratio. Therefore, despite a considerable effect on the pulse used, the impact of the probe and filter on the relative efficiencies of FAM-N and single conversion pulses is not very significant. However, it is possible that the efficiency of the single pulse, which can be easily reoptimised experimentally, could be improved, while this cannot be easily achieved for FAM-N. The final column of Table 3 shows the enhancement ratios obtained using FAM-N pulses affected by the filter (*i.e.*, the same efficiency as in the column headed Filter), but where the single pulse efficiency is returned to the maximum obtained previously (*i.e.*, an "ideal" case). The values are closer to those obtained experimentally. In general, the ability to easily optimise a single pulse experimentally and, therefore, account for any experimental imperfections that may be present, may go some way to explaining the differences between experiment and theory shown in Table 1.

In general, Table 3 reveals that the most important parameter to include when optimising a FAM-N pulse is C_Q, and while good enhancements are achieved over a wide range of C_Q values, if an estimate of C_Q is available this will provide a considerable advantage. Most other changes considered produce only a small loss in signal, although inclusion of η_Q has perhaps the most significant effect, suggesting that if this is known (or is similar for all sites present) it should be included in the optimisation. Although it seems including an estimation of the effects of relaxation (during the longer FAM-N pulse train), or the effects of pulse rise time, does not have a significant effect for $Na_4P_2O_7$, this might not be the case for all samples considered, and this may lead to differences between experimental and theoretical enhancements, particularly for I=3/2 where longer FAM-N pulses are typically produced.

4. Conclusions

FAM-N pulses provide an easily-implemented method for the improvement of the efficiency of multiple- to single-quantum conversion in MQMAS. The easy, automated high-throughput optimisation enables pulses to be generated rapidly, and these can be used without experimental reoptimisation, if required, providing signal enhancements typically between ×1.5 and ×5. In contrast to most previous methods, there are no restrictions on the pulse lengths that are considered in subsequent units, and the penultimate pulse is automatically reoptimised upon addition of the next, enabling a much wider variety of pulse trains to be considered. Most efficient pulses are generated when information on the MAS rate and rf field strength (both, in principle, under the control of the user) is included, and enhancements are improved if prior knowledge of the C_Q value (or at least a limit on this) is known. However, excellent signal enhancements have been observed when FAM-N pulses are applied to species with NMR parameters different from those for which they were optimised, and on samples with multiple (and different) species present, demonstrating their robust nature. Much less significant improvements in efficiency were observed upon the inclusion of η_Q values (although these could be included if known exactly). FAM-N pulses also display a good tolerance with respect to offset variation, with improved performance over a single pulse observed for offsets of ± 50 kHz (*i.e.*, under all conditions applicable to experiments at moderate-high field and

moderate-fast MAS).

We have also demonstrated in this work the applicability of FAM-N pulses at higher MAS rates (*i.e.*, up to 75 kHz), where it might have been expected that the longer pulse durations that result may lead to lower enhancements, but little variation was observed. The application of FAM-N pulses to nuclei with $I > 3/2$ was also shown, extending the initial work, and excellent enhancements were observed in all cases. However, it was noted that pulse trains tend to be shorter as I increases, reflecting the presence of multiple STs that may be affected by modulated pulses and many other transitions within the spin system to which coherences may be transferred. Application of FAM-N pulses to much more challenging systems, *i.e.*, those with low γ, low natural abundance, large second-order quadrupolar broadening and where only low rf field strengths are achievable was demonstrated. In these cases, experimental reoptimisation of any composite pulse is not possible (and indeed enhancement techniques may be required simply in order to acquire a spectrum). The robust nature of the FAM-N pulses, and the ability to obtain significant signal enhancement even when applied under varying conditions demonstrates they are a useful addition to the MQMAS approach, extending its potential application.

In general, the experimental enhancements achieved were in good agreement with those predicted theoretically, although best agreement was obtained for systems with $I > 3/2$, probably as a result of the shorter pulse trains that result. Differences between experiment and calculation for I=3/2 nuclei were investigated more thoroughly for ^{23}Na NMR of $Na_4P_2O_7$, which contains four distinct Na species, with the effect of applying an ideal FAM-N pulse to species with different C_Q, η_Q and δ_{iso} considered. Although a variation in efficiency is observed, the theoretical enhancement remains considerably higher than that seen experimentally. Little effect was observed upon the inclusion of the effects of differential T_2 relaxation (estimated from the linewidths in the indirect dimension of MQMAS experiments). However, the effects of the probe itself (*i.e.*, simulating the rise time of the pulse using a transfer function that models the probe as a filter) did produce a more significant change in the FAM-N efficiency. Although a drop in the efficiency of single-pulse conversion was also observed, resulting in a similar theoretical enhancement ratio, it is much easier to account for this experimentally, restoring optimum transfer efficiency, suggesting this is the origin of the differences observed between experiment and theoretical predictions (particularly for the longer pulse trains with shorter units observed for I=3/2 systems).

It should be noted that although we have chosen to automate the optimisation of a specific type of pulse, in principle, optimal control theory [68] provides much greater flexibility for optimising systems that exhibit many degrees of freedom. This has been employed in NMR spectroscopy to replace traditional hard pulses with flexible waveforms essentially consisting of a large number of short pulses of variable phase and amplitude. Although applied to date in MQMAS only for triple-quantum excitation [31], this approach has been used for population transfer prior to the application of a CT selective pulse [69], conceptually similar to the coherence transfer process in multiple-quantum conversion. The complexity of the optimisation may result in global solutions becoming increasingly difficult to identify as the variable space over which the search is performed increases, in contrast to the FAM-N approach considered here where simplicity is the primary aim. However, optimal control theory may offer interesting possibilities for future development.

Although STMAS experiments offer significant sensitivity gains over MQMAS (*e.g.*, factors of 2–5), the more difficult experimental implementation of this approach, and its sensitivity to higher-order effects (*e.g.*, third-order quadrupolar interactions) and microsecond-timescale dynamics, does ensure that there is still a need for more sensitive MQMAS experiments. We believe FAM-N pulses offer a simple, robust and efficient approach for the improvement of MQMAS experiments and will enable an increase in their applicability to more challenging, but more important and more interesting, systems.

Acknowledgements

We would like to thank EPSRC (EP/K503162/1) for the award of a studentship to HFC and the ERC (EU FP7 Consolidator Grant 614290 “EXONMR”) for support. SEA would also like to thank the Royal Society and Wolfson Foundation for a merit award. The UK 850 MHz solid-state NMR Facility used in this research was funded by EPSRC and BBSRC (contract reference PR140003), as well as the University of Warwick including *via* part funding through Birmingham Science City Advanced Materials Projects 1 and 2 supported by Advantage West Midlands (AWM) and the European Regional Development Fund (ERDF). Collaborative assistance from the 850 MHz Facility Manager (Dinu Iuga, University of Warwick) is acknowledged. Financial support from the TGIR-RMN-THC Fr3050 CNRS to access the 800 MHz spectrometer (Lille) is gratefully acknowledged, as is assistance from Julien Trebosc. The research data (and/or materials) supporting this publication can be accessed at DOI: 10.17630/21145f4d-39fa-4e63-8f21-eb613175da60.

Appendix A. Supplementary material

Supplementary data associated with this article can be found in the online version at http://dx.doi.org/10.1016/j.ssnmr.2017.01.001.

References

[1] K.J.D. MacKenzie, M.E. Smith, Multinuclear Solid-State NMR of Inorganic Materials, Pergamon Press, Oxford, 2002.
[2] S.E. Ashbrook, D.M. Dawson, J.M. Griffin, Solid-state NMR spectroscopy, in: D.W. Bruce, D. O'Hare, R.I. Walton (Eds.), Local Structural Characterisation, John Wiley & Sons Ltd, Chichester, 2014.
[3] R.E. Wasylishen, S.E. Ashbrook, S. Wimperis (Eds.), NMR of Quadrupolar Nuclei in Solid Materials, John Wiley & Sons Ltd., Chichester, 2012.
[4] A. Llor, J. Virlet, Towards high-resolution NMR of more nuclei in solids – sample spinning with time-dependent spinner axis angle, J. Chem. Phys. Lett. 152 (1988) 248–253.
[5] A. Samoson, E. Lippmaa, A. Pines, High resolution solid-state NMR, Mol. Phys. 65 (1988) 1013–1018.
[6] L. Frydman, J.S. Harwood, Isotropic spectra of half-integer quadrupolar spins from bidimensional magic-angle-spinning NMR, J. Am. Chem. Soc. 117 (1995) 5367–5368.
[7] S.P. Brown, S. Wimperis, Two-dimensional multiple-quantum MAS NMR of quadrupolar nuclei: a comparison of methods, J. Magn. Reson. 128 (1997) 42–61.
[8] A. Goldburt, P.K. Madhu, Multiple-quantum magic-angle spinning: high-resolution solid-state NMR of half-integer spin quadrupolar nuclei, Ann. Rep. NMR Spectrosc. 54 (2005) 81–153.
[9] J. Rocha, C.M. Morais, C. Fernandez, Progress in multiple-quantum magic-angle spinning NMR spectroscopy, Top. Curr. Chem. 246 (2005) 141–194.
[10] J. Kanellopoulos, D. Freude, A.P.M. Kentgens, Practical comparison of MQMAS techniques, Solid State Nucl. Magn. Reson. 32 (2007) 99–108.
[11] J.P. Amoureux, C. Fernandez, L. Frydman, Optimized multiple-quantum magic-angle spinning NMR experiments on half-integer quadrupoles, Chem. Phys. Lett. 259 (1996) 347–355.
[12] J.P. Amoureux, C. Fernandez, Triple, quintuple and higher order multiple quantum MAS NMR of quadrupolar nuclei, Solid State Nucl. Magn. Reson. 10 (1998) 211–223.
[13] J.P. Amoureux, M. Pruski, D.P. Lang, C. Fernandez, The effect of RF power and spinning speed on MQMAS NMR, J. Magn. Reson. 131 (1998) 170–175.
[14] Z. Gan, Isotropic NMR spectra of half-integer quadrupolar nuclei using satellite transitions and magic-angle spinning, J. Am. Chem. Soc. 122 (2000) 3242–3243.
[15] S.E. Ashbrook, S. Wimperis, High-resolution NMR of quadrupolar nuclei in solids: the satellite-transition magic angle spinning (STMAS) experiment, Prog. Nucl. Magn. Reson. Spectrosc. 45 (2004) 53–108.
[16] S.E. Ashbrook, A.J. Berry, W.O. Hibberson, S. Steuernagel, S. Wimperis, High-resolution ^{17}O NMR spectroscopy of Wadsleyite (β-Mg_2SiO_4), J. Am. Chem. Soc. 125 (2003) 11824–11825.
[17] S. Antonijevic, S.E. Ashbrook, S. Biedesek, R.I. Walton, S. Wimperis, H.X. Yang, Dynamics on the microsecond timescale in microporous aluminophosphate AlPO-14 as evidenced by ^{27}Al MQMAS and STMAS NMR spectroscopy, J. Am. Chem. Soc. 128 (2006) 8054–8062.
[18] J. Trebosc, J.P. Amoureux, Z. Gan, Comparison of high-resolution solid-state NMR MQMAS and STMAS methods for half-integer quadrupolar nuclei, Solid State Nucl. Magn. Reson. 31 (2007) 1–9.
[19] Z. Gan, H.-T. Kwak, Enhancing MQMAS sensitivity using signals from multiple coherence transfer pathways, J. Magn. Reson. 168 (2004) 346–351.

[20] J.P. Amoureux, L. Delevoye, S. Steuernagel, Z. Gan, S. Ganapathy, L. Montagne, Increasing the sensitivity of 2D high-resolution NMR methods applied to quadrupolar nuclei, J. Magn. Reson. 172 (2005) 268–278.
[21] A.P.M. Kentgens, R. Verhagen, Advantages of double frequency sweeps in static, MAS and MQMAS NMR of Spin I=3/2 nuclei, Chem. Phys. Lett. 300 (1999) 435–443.
[22] P.K. Madhu, A. Goldbourt, L. Frydman, S. Vega, Sensitivity enhancement of the MQMAS NMR experiment by fast amplitude modulation of the pulses, Chem. Phys. Lett. 307 (1999) 41–47.
[23] P.K. Madhu, A. Goldbourt, L. Frydman, S. Vega, Fast radio-frequency amplitude modulation in multiple-quantum magic-angle-spinning nuclear magnetic resonance: theory and experiments, J. Chem. Phys. 112 (2000) 2377–2391.
[24] A. Goldburt, P.K. Madhu, S. Vega, Enhanced conversion of triple to single-quantum coherence in the triple-quantum MAS NMR spectrosocopy of Spin-5/2 nuclei, Chem. Phys. Lett. 320 (2000) 448–456.
[25] R. Siegel, T.T. Nakashima, R.E. Wasylishen, Sensitivity enhancement of MQMAS NMR spectra of Spin 3/2 nuclei using hyperbolic secant pulses, Chem. Phys. Lett. 403 (2005) 353–358.
[26] M. Pruski, J.W. Wiench, J.P. Amoureux, On the conversion of triple- to single-quantum coherences in MQMAS NMR, J. Magn. Reson. 147 (2000) 286–295.
[27] T.J. Ball, S. Wimperis, Use of SPAM and FAM pulses in high-resolution MAS NMR spectroscopy of quadrupolar nuclei, J. Magn. Reson. 187 (2007) 343–351.
[28] G. Wu, D. Rovnyak, R.G. Griffin, Quantitative multiple-quantum magic-angle-spinning NMR spectroscopy of quadrupolar nuclei in solids, J. Am. Chem. Soc. 118 (1996) 9326–9332.
[29] T. Vosegaard, P. Florian, D. Massiot, P.J. Grandinetti, Multiple quantum magic-angle spinning using rotary resonance excitation, J. Chem. Phys. 114 (2001) 4618–4624.
[30] B. Koczor, J. Rohonczy, A novel pulse scheme for multiple quantum excitation, SFAM to enhance the sensitivity of MQMAS experiments, Solid State Nucl. Magn. Reson. 74 75 (2016) 1–9.
[31] T. Vosegaard, C. Kehlet, N. Khaneja, S.J. Glaser, N.C. Nielsen, Improved excitation schemes for multiple-quantum magic-angle spinning for quadrupolar nuclei designed using optimal control theory, J. Am. Chem. Soc. 127 (2005) 13768–13769.
[32] H.Y. Carr, E.M. Purcell, Effects of diffusion on free precession in nuclear magnetic resonance experiments, Phys. Rev. 94 (1954) 630–638.
[33] S. Meiboom, D. Gill, Modified spin-echo method for measuring nuclear relaxation times, Rev. Sci. Instrum. 29 (1958) 688–691.
[34] F.H. Larsen, N.C. Nielsen, Effects of finite Rf pulses and sample spinning speed in multiple-quantum magic-angle spinning (MQ-MAS) and multiple-quantum quadrupolar carr-purcell-meiboom-gill magic-angle spinning (MQ-QCPMG-MAS) nuclear magnetic resonance of half-integer quadrupolar nuclei, J. Phys. Chem. A 103 (1999) 10825–11083.
[35] M. Pruski, D.P. Lang, C. Fernandez, J.P. Amoureux, Multiple-quantum magic-angle spinning NMR with cross-polarization: spectral editing of high-resolution spectra of quadrupolar nuclei, Solid State Nucl. Magn. Reson 7 (1997) 327–331.
[36] S.E. Ashbrook, S. Wimperis, Multiple-quantum cross-polarization and two-dimensional MQMAS NMR of quadrupolar nuclei, J. Magn. Reson. 147 (2000) 238–249.
[37] H. Colaux, D.M. Dawson, S.E. Ashbrook, Efficient amplitude-modulated pulses for triple-to single-quantum coherence conversion in MQMAS NMR, J. Phys. Chem. A 118 (2014) 6018–6025.
[38] C.M. Morais, M. Lopes, C. Fernandez, J. Rocha, Assessing the potential of fast amplitude modulation pulses for improving triple-quantum magic angle spinning NMR spectra of half-integer quadrupolar nuclei, Magn. Reson. Chem. 41 (2003) 679–688.
[39] D. Massiot, B. Touzo, J.P. Trumeau, J. Virlet, P. Florian, P.J. Grandinetti, Two-dimensional magic-angle spinning isotropic reconstruction sequences for quadrupolar nuclei, Solid State Nucl. Magn. Reson. 6 (1996) 73–83.
[40] M. Bak, J. Rasmussen, N. Nielsen, SIMPSON: a general simulation program for solid-state NMR spectroscopy, J. Magn. Reson. 147 (2000) 296–330.
[41] MATLAB Release 2011b, The MathWorks, Inc., Natick, Massachusetts, United States.
[42] S.P. Brown, S. Wimperis, Two-dimensional multiple-quantum MAS NMR of quadrupolar nuclei. acquisition of the whole echo, J. Magn. Reson. 124 (1997) 279–285.
[43] R. Tabeta, H. Saito, ^{23}Na chemical shifts of some inorganic and organic compounds in the solid state as determined by the magic angle spinning and high power NMR methods, Chem. Lett. 13 (1984) 293–296.
[44] R. Dupree, M.E. Smith, Solid-state magnesium-25 NMR spectroscopy, J. Chem. Soc. Chem. Commun. (1988) 1483–1485.
[45] P.J. Barrie, Distorted powder lineshapes in ^{27}Al CP MAS NMR spectroscopy of solids, J. Phys. Chem. A 102 (1998) 9750–9760.
[46] K.E. Johnston, M.R. Mitchell, F. Blanc, P. Lightfoot, S.E. Ashbrook, Structural study of $La_{1-x}Y_xScO_3$, combining neutron diffraction, solid-state NMR, and first-principles DFT calculations, J. Phys. Chem. C 117 (2013) 2252–2265.
[47] O.B. Lapina, D.F. Khabibulin, K.V. Romanenko, Z. Gan, M. Zuev, V.N. Krasil'nikov, V.E. Fedorov, ^{93}Nb NMR chemical shift scale for Niobia systems, Solid State Nucl. Magn. Reson. 28 (2005) 204–224.
[48] K.J. Pike, R.P. Malde, S.E. Ashbrook, J. McManus, S. Wimperis, Multiple-quantum MAS NMR of quadrupolar nuclei. Do five-, seven- and nine-quantum experiments yield higher resolution than the three-quantum experiment?, Solid State Nucl. Magn. Reson. 16 (2000) 203–215.
[49] S.E. Ashbrook, S. Wimperis, Spin-locking of half-integer quadrupolar nuclei in nuclear magnetic resonance of solids: second-order quadrupolar and resonance offset effects, J. Chem. Phys. 131 (2009) 194509.
[50] G. Engelhardt, A.P.M. Kentgens, H. Koller, A. Samoson, Strategies for extracting NMR parameters from ^{23}Na MAS, DOR and MQMAS spectra. A case study for $Na_4P_2O_7$, Solid State Nucl. Magn. Reson. 15 (1999) 171–180.
[51] F. Perras, I. Korobkov, D.L. Bryce, NMR crystallography of sodium diphosphates: combining dipolar, shielding, quadrupolar, diffraction, and computational information, CrystEngComm 15 (2013) 8727–8738.
[52] S.E. Ashbrook, S. Wimperis, High-resolution NMR spectroscopy of quadrupolar nuclei in solids: satellite-transition MAS with self-compensation for magic-angle misset, J. Am. Chem. Soc. 124 (2002) 11602–11603.
[53] F.H. Larsen, I. Farnan, Site populations and short range order in aluminosilicates investigated by ^{27}Al solid-state NMR, J. Phys. Chem. B 108 (2004) 9764–9771.
[54] N. Kim, C.-H. Hsieh, J.F. Stebbins, Scandium coordination in solid oxides and stabilized zirconia: ^{45}Sc NMR, Chem. Mater. 18 (2006) 3855–3859.
[55] K.E. Johnston, J.M. Griffin, R.I. Walton, D.M. Dawson, P. Lightfoot, S.E. Ashbrook, ^{93}Nb NMR and DFT investigation of the polymorphs of $NaNbO_3$, Phys. Chem. Chem. Phys. 13 (2011) 7565–7576.
[56] K.E. Johnston, C.C. Tang, J.E. Parker, K.S. Knight, P. Lightfoot, S.E. Ashbrook, The polar phase of $NaNbO_3$: a combined study by powder diffraction, solid-state NMR, and first-principles calculation, J. Am. Chem. Soc. 132 (2010) 8732–8746.
[57] M. Amri, S.E. Ashbrook, D.M. Dawson, J.M. Griffin, R.I. Walton, S. Wimperis, A multinuclear solid-state NMR study of templated and calcined chabazite-type GaPO-34, J. Phys. Chem. C 116 (2012) 15048–15057.
[58] D. Massiot, T. Vosegaard, N. Magneron, D. Trumeau, V. Montouillout, P. Berthet, T. Loiseau, B. Bujoli, ^{71}Ga NMR of reference Ga_{IV}, Ga_V, and Ga_{VI} compounds by MAS and QPASS, extension of gallium/aluminum NMR parameter correlation, Solid State Nucl. Magn. Reson. 15 (1999) 159–169.
[59] L.B. Alemany, S. Steuernagel, J.P. Amoureux, R.L. Callender, A.R. Barron, Very fast MAS and MQMAS NMR studies of the spectroscopically challenging minerals kyanite and andalusite on 400, 500, and 800 MHz spectrometers, Solid State Nucl. Magn. Reson. 14 (1999) 1–18.
[60] Z. Gan, P. Srinivasan, J.R. Quine, S. Steuernagel, B. Knott, Third-order effect in solid-state NMR of quadrupolar nuclei, Chem. Phys. Lett. 367 (2003) 163–169.
[61] S.E. Ashbrook, S. Wimperis, SCAM-STMAS: satellite-transition MAS NMR of quadrupolar nuclei with self-compensation for magic-angle misset, J. Magn. Reson. 162 (2003) 402–416.
[62] N.G. Dowell, S.E. Ashbrook, S. Wimperis, Satellite-transition MAS NMR of low-γ nuclei at natural abundance: sensitivity, practical implementation, and application to ^{39}K (I=3/2) and ^{25}Mg (I=5/2), J. Phys. Chem. B 108 (2004) 13292–13299.
[63] T.J. Bastow, Powder determination of ^{39}K nuclear quadrupole coupling, J. Chem. Soc. Faraday Trans. 87 (1991) 2453–2455.
[64] S.E. Ashbrook, J.M. Griffin, Solid-state NMR of high-pressure silicates in the Earth's mantle, Ann. Rep. NMR Spectrosc. 79 (2013) 242–332.
[65] B. Derighetti, S. Hafner, H. Marxer, H. Rager, NMR of ^{29}Si and ^{25}Mg in Mg_2SiO_4 with dynamic polarization technique, Phys. Lett. A 66 (1978) 150–152.
[66] B. Winkler, P. Blaha, K. Schwarz, *Ab Initio* calculation of electric-field-gradient tensors of forsterite, Am. Mineral. 81 (1996) 545–549.
[67] M.C. Davis, W.J. Brouwer, A.S. Lipton, Z. Gan, K.T. Mueller, Characterization of cation environments in polycrystalline forsterite by ^{25}Mg MAS, MQMAS, and QCPMG NMR, Am. Mineral. 95 (2001) 1601–1607.
[68] L. Pontryagin, B. Boltyanskii, R. Gamkreldze, E. Mishchenko, The Mathematical Theory of Optimal Processes, Wiley-Interscience, New York, 1962.
[69] L.A. O'Dell, C.I. Ratcliffe, Crystal structure based design of signal enhancement schemes for solid-state NMR of insensitive half-integer quadrupolar nuclei, J. Phys. Chem. A 115 (2011) 747–752.